

# A toy model of a protein prototype reveals nontrivial ultrametricity of the energy landscape

A. Kh. Bikulov

*N.N. Semenov Federal Research Center for Chemical Physics,  
Russian Academy of Sciences,  
Kosygin street 4, 117734 Moscow, Russia  
e-mail: beecul@mail.ru*

and

A. P. Zubarev

*Volga State Transport University,  
Pervyi Bezymyannyi pereulok 18, Samara, 443066, Russia;  
Samara University,  
Moskovskoe shosse 34, Samara, 443123 Russia  
e-mail: apzubarev@mail.ru*

March 16, 2026

## Abstract

This work presents a theoretical and computational framework for investigating the ultrametricity of the energy landscape in a model of a disordered heteropolymer. This model is considered as the toy model of a protein molecule, in which amino acid residues are modeled as material points. In this model, pairwise interactions include universal repulsion, the Lennard-Jones potential for hydrophobic residues, the Coulomb potential with screening for charged residues, and an elastic potential for bonds between neighboring residues. In studying this model, we employ its analogy with spin glass models, which allows the application of replica theory methods for the statistical description of the system. However, in contrast to the standard approach to disordered systems, averaging over disorder (over different sequences) is not performed. Each sequence is analyzed independently, which is necessary for understanding how a specific realization of disorder influences the formation of hierarchical structure. In this case, the overlap between replicas is defined as the Pearson correlation coefficient between vectors of mean pairwise energies, which corresponds to comparing thermodynamic averages in the spirit of spin glass theory. The paper presents the results of a computational experiment conducted using a developed algorithm on a GPU. The simulation used a chain of length  $N = 128$  residues,  $K = 50$  independent disorder realizations,  $M = 50$  replicas for each sequence at temperature  $T = 1.0$  in arbitrary units, and potentials with fixed parameters. It was found that for 90.0% of sequences, the distance matrix between

replicas contains more than half of ultrametric triangles, and in the vast majority of such cases (97.8%), nontrivial ultrametricity predominates, providing evidence for the hierarchical organization of the energy landscape even within this extremely simplified model. A repeated computational experiment for selected sequences confirms the robustness of the observations: 95.5% of them again demonstrated ultrametricity, of which 97.7% exhibited predominance of the nontrivial type of ultrametricity. The obtained results support Frauenfelder’s hypothesis about the ultrametricity of proteins and open the way for a systematic study of ultrametric properties in more realistic protein models.

## 1 Introduction

The concept of ultrametricity entered physics from mathematics, specifically from number theory and functional analysis. In contrast to the Euclidean metric, an ultrametric  $d$  satisfies the so-called strong triangle inequality: for any three points  $x, y, z$ , the condition  $d(x, z) \leq \max\{d(x, y), d(y, z)\}$  holds. Consequently, this modification of the axiomatic definition of a metric leads to several important consequences: in an ultrametric space, all triangles are isosceles with the base no longer than the equal sides, and any two balls are either disjoint or one is completely contained within the other. Such a structure is ideally suited for describing hierarchical systems, where the states of a system can be represented as a branching tree: the distance between two leaves is determined by the level of their nearest common ancestor. It is precisely this property that has made ultrametricity a key concept in describing systems with complex energy landscape structure — from spin glasses to biological macromolecules.

The discovery of ultrametricity in condensed matter physics is inextricably linked to the theory of spin glasses. Spin glasses are magnetic systems with competing ferromagnetic and antiferromagnetic interactions, leading to frustrations and a huge number of nearly degenerate ground states. For a long time, the description of such systems remained an unsolvable problem until 1979, when Parisi proposed a solution method for the Sherrington–Kirkpatrick (SK) model by introducing an infinite number of order parameters and the concept of spontaneous replica symmetry breaking [1, 2]. Soon after Parisi’s work, it was realized that the hierarchy of order parameters has a direct geometric interpretation [3, 4]. Namely, it was shown that the space of pure states in a spin glass possesses an ultrametric structure: overlaps (correlations) between states satisfy the strong triangle inequality, and the states themselves can be organized into a hierarchical tree. Subsequently, the development of various methods for proving ultrametricity in spin glasses proceeded along two directions: theoretical and computational. On the theoretical side, the works of Talagrand played a key role, providing rigorous mathematical foundations for Parisi’s ideas [5, 6, 7]. These works proved the Parisi formula for the free energy of the SK model and laid the foundations for a rigorous approach to ultrametricity. These ideas were further developed in the works of Panchenko, who proved that ultrametricity is not merely a possible but a necessary property of generalized SK models under certain symmetry conditions [8, 9, 10]. Contemporary research in this direction continues. For example, a recent work by Subag [11] develops the Thouless–Anderson–Palmer (TAP) approach and shows how the ultrametric tree of pure states can be naturally embedded into the configuration space of spherical models, with points on this tree approximately satisfying TAP equations for critical points.

Numerical studies of ultrametricity in spin glasses have been conducted in parallel with theoretical ones. Monte Carlo simulations for the three-dimensional Edwards–Anderson model, performed in a series of works (see, e.g., [12, 13, 14, 15]), confirmed the presence of hierarchical organization of states and ultrametric properties of the overlap distribution. Later, with the growth of computational power, works appeared that directly tested the ultrametric inequality for configurations obtained from simulated annealing (see, e.g., [16]). These studies confirmed that in the spin glass phase, overlap triangles are indeed isosceles, with deviations from ultrametricity disappearing as temperature decreases and system size increases. Modern numerical experiments on supercomputers (see, e.g., [17]) continue to investigate the limits of applicability of the ultrametricity hypothesis and its connection with dynamical properties such as aging and slow relaxation. These studies show that ultrametricity manifests not only in equilibrium properties but also in nonequilibrium dynamics, where the system hierarchically explores the valleys of the energy landscape. It is also interesting to note that recent experimental work on photonic analogs of spin glasses (random lasers) has confirmed the existence of ultrametric structure in real physical systems [18], demonstrating the universality of this phenomenon.

The success of the ultrametric approach in spin glass physics has influenced related fields, particularly biophysics. More than forty years ago, Frauenfelder hypothesized the ultrametric nature of proteins. The basis for this hypothesis was a series of experiments on carbon monoxide (CO) binding to myoglobin [19, 20, 21]. In these experiments, a myoglobin sample with bound CO was irradiated with a laser pulse, breaking the bond, and then the kinetics of rebinding were observed over a wide range of time scales — from nanoseconds to hundreds of seconds — and over a broad temperature interval (from 60 to 300 K). As a result of these experiments, it was discovered that the kinetics of CO binding to myoglobin are strongly nonexponential, with the shape of the curves depending on temperature in a complex manner. Frauenfelder suggested that a protein could exist in many different metastable substates organized hierarchically: substates separated by small energy barriers are combined into clusters separated by higher energy barriers, these clusters are combined into even larger clusters, and so on. Such a hierarchical structure is naturally described by an ultrametric tree, and protein dynamics can be described as a random walk on this ultrametric tree [22].

Attempts to prove the existence of ultrametricity in protein states can be divided into three categories: theoretical modeling, analysis of experimental data, and computational experiments in protein models. The most consistent program for theoretical modeling of protein dynamics within the ultrametric framework was developed in [23, 24, 25, 26], where the apparatus of  $p$ -adic analysis was proposed to describe protein conformational dynamics. In this approach, the set of metastable states (conformation space) of a protein is described by an ultrametric space, which is taken to be the set of  $p$ -adic numbers (or some subset thereof), and diffusion through this space is described by  $p$ -adic pseudodifferential equations. In [24, 25, 26], it was shown that the same model of ultrametric diffusion with a reactive sink describes the kinetics of CO binding to myoglobin over the entire temperature range from 60 to 300 K. At high temperatures (200–300 K), the model predicts power-law kinetics at the initial stage, transitioning to an exponential, while at low temperatures (below 180 K), it predicts a purely power-law dependence, which exactly corresponds to experimental observations. This result can be considered strong indirect evidence in favor of the

ultrametric organization of proteins, since no other model has so far been able to uniformly describe the data over the entire range of times and temperatures.

Direct experimental proof of protein ultrametricity has long remained unattainable due to limitations in spatiotemporal resolution. However, a recent breakthrough in super-resolution microscopy has opened new perspectives. For example, work [27] demonstrates the possibility of visualizing individual protein shapes with approximately 1 nanometer resolution using one-step nanoscale expansion microscopy. Although this work does not directly measure ultrametricity, it shows that experimental observation of conformational landscapes at the single-molecule level is becoming a reality, which may in the future allow direct testing of ultrametric hypotheses.

In the field of computational experiments, there is also some work providing evidence in favor of protein ultrametricity. For example, the authors of [28] conducted a computer study of the conformational space of the poly-L-alanine peptide consisting of 20 residues, using an all-atom model. Using molecular dynamics and Monte Carlo methods, they generated an ensemble of conformations, then performed minimization to search for local energy minima. The main goal of the work was to test the hypothesis that the protein energy landscape, like that of spin glasses, possesses the property of ultrametricity. As a result, the authors found that the set of low-energy conformations (alpha-helices) indeed exhibits an ultrametric structure, indicating the presence of hierarchical organization among states close in energy. There are also later works in the framework of molecular dynamics that provide direct or indirect evidence in favor of protein ultrametricity. In [29], the possibility of applying an ultrametric approach to the analysis of protein folding kinetics was investigated. The authors of this work used ergodic Markov state models constructed from molecular dynamics trajectories and showed that the free energy of the transition state between two nodes, defined through the minimum cut, satisfies the axioms of ultrametricity. This allowed the development of an automatic procedure for reducing the model to a small number of macrostates, with the resulting rate constants having clear physical meaning and agreeing with transition state theory and Kramers' theory. This work provides strong computational confirmation that the conformation space of proteins indeed possesses an ultrametric topology. Another direction of computational research is represented by [30]. Here, the authors applied an information-theoretic approach based on the concepts of resolution and relevance to assess the quality of various methods for clustering protein conformational space. They investigated seven different hierarchical clustering strategies on a molecular dynamics dataset for twelve structurally different proteins. The results showed that the most physically adequate clusterings are those that preserve the ultrametric structure of the low-dimensional space. This study is interesting because it does not postulate ultrametricity but rather discovers it as a natural property of optimal clusterings, which serves as independent confirmation of Frauenfelder's hypothesis.

The present work lies at the intersection of theoretical modeling and computational experiments in models of disordered polymers, which we consider as models of protein prototypes. We consider a simple model of a polymer chain with four types of residues, describe a theoretical and computational scheme for investigating the ultrametricity of the energy landscape of such a system, and conduct a computational experiment to study ultrametricity in this model. This model represents an abstract system consisting of a chain of point particles (by analogy with real proteins we call them "residues"), sequentially connected by

elastic forces, and can be considered only as a highly simplified version of some prototype of a polypeptide chain. Residues are classified into four types: hydrophobic, hydrophilic positively charged, hydrophilic negatively charged, and hydrophilic neutral. For all pairs of residues, short-range repulsion exists. Hydrophobic residues interact pairwise via the Lennard-Jones potential. Charged hydrophilic residues interact via the Coulomb potential. Additionally, all residues that are neighbors in the chain interact via an elastic potential.

It is important to emphasize that the proposed model is not a model of any specific protein. By the term "protein prototype model" we understand an abstract mathematical construction that imitates only the most general features of protein macromolecules: a linear sequence of different monomers (residues) and the presence of interactions qualitatively resembling hydrophobic and electrostatic forces. This model represents an extremely simplified, or "toy," system intended for investigating fundamental statistical properties of the energy landscape, rather than for quantitative description of real proteins. All elements of the model (point particles, interaction potentials) are chosen so that, on the one hand, key factors leading to frustration and complex landscape (competition between attraction and repulsion, diversity of monomer types) are preserved, while on the other hand, computational complexity is minimized, making statistical analysis possible using methods analogous to spin glass theory. This approach fully corresponds to the spirit of "toy models" in condensed matter physics, where the main goal is to identify qualitative patterns rather than achieve chemical accuracy.

In constructing and analyzing the model, we use the analogy with spin glass theory, which allows employing the apparatus of replica theory for statistical analysis of the system. The analysis we apply is based on the use of concepts of disorder (specific residue sequence), microstates (specific spatial configurations), and macrostates (replicas as canonical distributions of configurations). This enables statistical averaging both over thermal fluctuations and over the ensemble of different sequences. Nevertheless, the analysis of ultrametricity is performed for each sequence separately, without averaging the overlap matrices over disorders. To investigate ultrametricity, we use a computational algorithm including the following stages: generation of an ensemble of random residue sequences (disorder realizations); achievement of thermal equilibrium for each sequence by the Monte Carlo method with the Metropolis algorithm [32, 33], simulated annealing, and individual step-size adaptation for each replica; collection of statistically independent configurations for constructing canonical distributions (replicas); computation of the overlap matrix between replicas based on comparison of pairwise energy distributions; verification of ultrametricity of the obtained distance matrix separately for each sequence.

It should be noted that when verifying ultrametricity, one should distinguish between so-called "trivial ultrametricity" and "nontrivial ultrametricity." Trivial ultrametricity occurs when distances between any three points are equal. Such ultrametricity can arise in systems without real hierarchy, for example, with random selection of points in a high-dimensional space [34, 35]. Nontrivial ultrametricity, on the contrary, is convincing evidence of a complex hierarchical organization of the state space. It is precisely the distinction between these cases that is of fundamental importance for the correct interpretation of the results of our computational experiment. Furthermore, it is also necessary to take into account the fact that in models of non-ergodic systems, such as spin glasses and proteins, different initial microstates during Monte Carlo simulation may converge to the same macrostate (replica).

Namely, upon random initialization of system configurations, some configurations may over time fall into the basin of attraction of the same macrostate, leading to high overlap values (close to unity) between the corresponding replicas. For a correct analysis of ultrametricity, one should consider only those replicas that are guaranteed to belong to different macrostates. Therefore, it is also necessary to use a procedure for selecting unique replicas: if the overlap between two replicas exceeds a given threshold, they are considered to belong to the same macrostate, and one of them is excluded from further consideration. Thus, the analysis of ultrametricity is performed only on the set of replicas corresponding to different macrostates, which allows correctly identifying the hierarchical structure, if it exists.

It is important to emphasize the conceptual difference between the approach adopted in this work and the classical approach to disordered polymers. From a formal point of view, our model with a fixed but random residue sequence is a typical example of a disordered heteropolymer. In condensed matter physics, the standard procedure for such systems is averaging all observables over the ensemble of disorder realizations (sequences), which allows obtaining a description of the typical behavior of the system. However, in the context of protein research, such an approach is not adequate. Each real protein is a specific sequence, and its unique properties, including the structure of its energy landscape, are determined precisely by this specificity. Therefore, in contrast to the classical theory of disordered polymers, in this work we fundamentally refrain from averaging over disorder. All stages of analysis — from constructing overlap matrices to classifying types of ultrametricity — are performed for each sequence (for each disorder realization) independently. This allows not only estimating the fraction of sequences demonstrating hierarchical organization but also, in perspective (when transitioning to more realistic models), studying which specific features of the amino acid sequence encode the complexity of the energy landscape, which directly brings us closer to understanding the principles of folding and functioning of real proteins.

The work is organized as follows. Section 2 presents a complete description of our proposed toy model of a protein prototype. Section 3 describes in detail the algorithm for investigating ultrametricity, including all computational stages and statistical procedures. Section 4 presents the simulation results, revealing nontrivial ultrametricity in the considered model. The final section presents concluding remarks and discussion of prospects for further research.

## 2 Description of the toy model of a protein prototype for studying ultrametricity

In our model, a protein prototype is considered as a linear chain consisting of  $N$  ordered material points, in which neighboring points are connected by linear elastic forces. By analogy with proteins, we will also call these material points amino acid residues. From a formal point of view, such a system represents a classic example of a disordered heteropolymer: a linear chain consisting of monomers (residues) of several types, whose sequence along the chain is fixed but random. In real proteins, residues differ in their chemical properties, which determines the specificity of their interactions. In our model, we use a simplified classification including four types of residues: hydrophobic, hydrophilic positively charged, hydrophilic negatively charged, and hydrophilic neutral. This division allows accounting not only for

the hydrophobic effect but also for electrostatic interactions, which play an important role in stabilizing protein structures and can generate additional frustrations.

Formally, the residue sequence is defined as a vector  $\sigma = (\sigma_1, \sigma_2, \dots, \sigma_N)$ , where each element  $\sigma_i$  encodes the residue type. We introduce two characteristics for each residue: charge  $q_i \in \{-1, 0, +1\}$  and hydrophobicity indicator  $h_i \in \{0, 1\}$ . Hydrophobic residues ( $h_i = 1, q_i = 0$ ) interact via the Lennard-Jones potential. Charged residues ( $q_i = \pm 1, h_i = 0$ ) participate in Coulomb interactions. Neutral hydrophilic residues ( $q_i = 0, h_i = 0$ ) have no specific interactions, except for universal repulsion.

The ensemble of different sequences  $\sigma^{(k)}_{k=1}^K$  constitutes the realization of disorder in the system, characteristic of disordered heteropolymers. However, as already noted in the Introduction, in contrast to the standard statistical mechanics of disordered systems, where averaging over this ensemble is performed, in this work each sequence  $k$  is considered as unique and analyzed separately. We consider  $K$  independent sequences, each generated randomly: each residue independently receives its corresponding type with given probabilities  $p_{\text{hp}}$  (hydrophobic),  $p_+$  (positive),  $p_-$  (negative), and  $p_{\text{neut}} = 1 - p_{\text{hp}} - p_+ - p_-$  (neutral). All sequences are considered equally probable.

A microstate of the system is considered to be a specific spatial configuration of the sequence. The configuration is specified by a set of residue coordinates  $R = \{r_1, r_2, \dots, r_N\}$ ,  $r_i \in \mathbb{R}^3$ . The energy function of the model has the form of a sum of several contributions:

$$E(R, \sigma) = \sum_{i < j} U_{\text{pair}}(r_{ij}, q_i, q_j, h_i, h_j) + \sum_{i=1}^{N-1} U_{\text{bond}}(r_{i,i+1}), \quad (1)$$

where  $r_{ij} = |\vec{r}_i - \vec{r}_j|$ , and  $q_i, h_i$  are determined by the residue type  $\sigma_i$ . The pairwise potential  $U_{\text{pair}}$  includes universal short-range repulsion, Lennard-Jones attraction potential, Coulomb potential, and elastic potential. The universal short-range repulsion acts for all pairs of residues regardless of their type:

$$U_{\text{rep}}(r_{ij}) = \begin{cases} \varepsilon_{\text{rep}} \left( \frac{\sigma_{\text{rep}}}{r_{ij}} \right)^{12}, & \text{if } r_{ij} < \sigma_{\text{rep}}, \\ 0, & \text{if } r_{ij} \geq \sigma_{\text{rep}}. \end{cases}$$

The Lennard-Jones attraction potential is taken into account only between hydrophobic residues ( $h_i = h_j = 1$ ) that are not nearest neighbors along the chain ( $|i - j| > 1$ ), at distances not exceeding the cutoff radius  $r_{\text{cut}}$ :

$$U_{\text{LJ}}(r_{ij}) = 4\varepsilon_{\text{LJ}} \left[ \left( \frac{\sigma_{\text{LJ}}}{r_{ij}} \right)^{12} - \left( \frac{\sigma_{\text{LJ}}}{r_{ij}} \right)^6 \right]. \quad (2)$$

The Coulomb potential is taken into account for all pairs of charged residues ( $q_i \neq 0, q_j \neq 0$ ), also excluding nearest neighbors. To avoid divergence at small distances, a minimum distance  $r_{\text{min}}$  is introduced, and Debye screening is also taken into account:

$$U_{\text{coul}}(r_{ij}) = \begin{cases} k_{\text{coul}} \frac{q_i q_j}{r_{ij}} \exp\left(-\frac{r_{ij}}{\lambda_{\text{Debye}}}\right), & r_{ij} \geq r_{\text{min}}, \\ k_{\text{coul}} \frac{q_i q_j}{r_{\text{min}}}, & r_{ij} < r_{\text{min}}. \end{cases} \quad (3)$$

Here  $k_{\text{coul}}$  is a constant determining the strength of electrostatics,  $\lambda_{\text{Debye}}$  is the screening length. Thus, the total pairwise potential for a pair  $(i, j)$  has the form:

$$U_{\text{pair}}(r_{ij}, q_i, q_j, h_i, h_j) = U_{\text{rep}}(r_{ij}) + \delta_{h_i, 1} \delta_{h_j, 1} \delta_{|i-j| > 1} U_{\text{LJ}}(r_{ij}) + \delta_{q_i \neq 0} \delta_{q_j \neq 0} \delta_{|i-j| > 1} U_{\text{coul}}(r_{ij}),$$

where we use the notation  $\delta_A = 1$  if condition  $A$  is satisfied and  $\delta_A = 0$  if condition  $A$  is not satisfied. The elastic potential  $U_{\text{bond}}$  acts between neighboring residues of the chain and ensures its integrity:

$$U_{\text{bond}}(r_{i,j}) = \frac{1}{2} k_{\text{bond}} (r_{i,j} - r_{\text{bond}})^2 \delta_{|i-j|=1}, \quad (4)$$

where  $r_{\text{bond}}$  is the equilibrium bond length,  $k_{\text{bond}}$  is the bond stiffness.

To characterize the state of the system, we use the concept of a pairwise energy vector. For each configuration  $R$ , a vector  $u \in \mathbb{R}^{N_p}$  is computed, where  $N_p = \frac{N(N-1)}{2}$  is the number of unique residue pairs  $(i < j)$ . The components of this vector are the values of the total pairwise potential  $U_{\text{pair}}$  for all pairs, including contributions from repulsion, Lennard-Jones, Coulomb, and elastic interactions. Thus, each configuration is mapped to a point  $u$  in the pairwise energy space of dimension  $N_p$ , and this point carries information about all interactions in the system.

A macrostate of the system is described by the canonical Gibbs distribution. For each fixed residue sequence  $\sigma^{(k)}$  (where  $k = 1, \dots, K$  is the index of the amino acid sequence (disorder realization)), the probability of finding the system in configuration  $R$  at temperature  $T$  is determined by the Boltzmann distribution:

$$P(R|\sigma^{(k)}) = Z^{-1}(\sigma^{(k)}) \exp(-\beta E((R, \sigma^{(k)})),$$

where  $\beta = \frac{1}{k_B T}$  is the inverse temperature,  $E((R, \sigma^{(k)}))$  is the energy of configuration  $R$  for sequence  $\sigma^{(k)}$ ,  $Z(\sigma^{(k)}) = \int dR \exp(-\beta E((R, \sigma^{(k)}))$  is the partition function. In the context of replica theory [1, 2, 3], such macrostates will be called replicas. Let  $m = 1, \dots, M$  be the replica index,  $s = 1, \dots, S$  be the index of a statistically independent realization of a microstate within a replica,  $R^{(k,m,s)}$  be the configuration corresponding to sequence  $k$ , replica  $m$ , and realization  $s$ . Then each replica  $m$  for sequence  $k$  is represented by a set of  $S$  statistically independent configurations  $\{R^{(k,m,s)}\}_{s=1}^S$ , sampled from the Boltzmann distribution. For a fixed amino acid sequence  $k$ , the set of all possible configurations  $R^{(k,m,s)}$  forms the phase space of the system.

The central point of our methodology is the definition of overlap between two replicas. As is known, in spin glass theory, the overlap between two replicas  $\alpha$  and  $\beta$  is defined through thermodynamic averages:

$$q^{\alpha\beta} = \frac{1}{N} \sum_{i=1}^N \langle s_i \rangle_\alpha \langle s_i \rangle_\beta,$$

where  $\langle s_i \rangle_\alpha$  is the average value of spin  $i$  over all configurations in replica  $\alpha$ , and  $N$  is the total number of spins. This definition is fundamentally important: it compares not

specific microstates but characteristics of distributions — the average magnetizations. In this case, the overlap  $q^{\alpha\beta}$  takes values in the interval  $[-1, 1]$ , which follows from the fact that the average magnetizations of individual spins  $\langle s_i \rangle_\alpha$  also lie in this interval. Drawing a direct analogy for our model, we introduce the following definition of overlap between replicas  $m$  and  $n$  for a fixed sequence  $k$ . For each replica, we compute the vector of mean pairwise energies  $\bar{u}^{(k,m)} \in \mathbb{R}^{N_p}$ , whose components are the thermodynamic averages of the total pairwise energy for each pair of residues:

$$\bar{u}_p^{(k,m)} = \langle u_p \rangle_{k,m} = \frac{1}{S} \sum_{s=1}^S u_p^{(k,m,s)},$$

where  $p = 1, \dots, N_p$  enumerates all unique pairs  $(i, j)$  with  $i < j$ .

To obtain a definition of overlap that (i) takes values in  $[-1, 1]$  as in spin glass theory, (ii) is invariant under linear transformations of the energy scale, and (iii) has a clear statistical interpretation as a measure of linear correlation between distributions, we use the Pearson correlation coefficient between the vectors of mean pairwise energies:

$$q_{mn}^{(k)} = \frac{\sum_{p=1}^{N_p} (\bar{u}_p^{(k,m)} - \bar{U}^{(k,m)}) (\bar{u}_p^{(k,n)} - \bar{U}^{(k,n)})}{\sqrt{\sum_{p=1}^{N_p} (\bar{u}_p^{(k,m)} - \bar{U}^{(k,m)})^2} \sqrt{\sum_{p=1}^{N_p} (\bar{u}_p^{(k,n)} - \bar{U}^{(k,n)})^2}}, \quad \bar{U}^{(k,m)} = \frac{1}{N_p} \sum_{p=1}^{N_p} \bar{u}_p^{(k,m)}. \quad (5)$$

The physical interpretation of this definition is as follows. If in two replicas the system spends time in configurations where the average interaction energies for each pair of residues are close (up to a linear transformation), then such replicas are considered similar, and their overlap is close to unity. If the distributions differ significantly (for example, in one replica configurations with strong attraction of hydrophobic residues dominate, while in another configurations with predominance of repulsion dominate), then the overlap will be small or even negative. The use of centering and normalization eliminates the influence of absolute energy values, leaving only information about the shape of the distributions.

After computing all pairwise overlaps for sequence  $k$ , an overlap matrix  $q_{mn}^{(k)}$  of dimension  $M \times M$  is formed. The distance matrix is defined through the correlation coefficient as  $D_{mn}^{(k)} = 1 - q_{mn}^{(k)}$ . This definition guarantees that  $D_{mn}^{(k)} \in [0, 2]$ , with  $D_{mn}^{(k)} = 0$  corresponding to identical distributions, and  $D_{mn}^{(k)} = 2$  corresponding to the maximum possible difference (anticorrelation). It is precisely these matrices, individual for each sequence, that are subjected to further analysis for ultrametricity. Averaging of the overlap matrices over the ensemble of sequences is not performed, as it would destroy information about the different types of energy landscapes inherent in different disorder realizations.

### 3 Algorithm for investigating the ultrametricity of the energy landscape

The algorithm we use represents a computational scheme for testing the presence of ultrametricity in the energy landscape of the protein prototype model described in the previous section. The algorithm consists of a sequence of stages, each implementing a specific physical or mathematical procedure. An important feature of the algorithm is its parallelizability: computations can be performed simultaneously for different disorder realizations (residue sequences) and for different replicas (independent thermal ensembles). This allows efficient use of modern computational resources, including graphics processing units.

Let us describe this algorithm stage by stage.

Stage 1. Generation of an ensemble of random residue sequences. At this stage, parameters are set: number of sequences  $K$ , chain length  $N$ , probabilities of three residue types  $p_{\text{hp}}$  (hydrophobic),  $p_+$  (hydrophilic positively charged),  $p_-$  (hydrophilic negatively charged); the probability of the fourth type (hydrophilic neutral) is computed automatically. Each sequence is generated independently using a fixed random number generator seed, which ensures reproducibility of results. For different sequences, different independent random streams are used, effectively implemented by the generator, but the overall seed is fixed. This stage corresponds to creating an ensemble of different sequences with a given composition but random order of residues.

Stage 2. Initialization of configurations for each sequence and each replica. At this stage, for each sequence  $\sigma^{(k)}$  ( $k = 1, \dots, K$ ),  $M$  independent replicas are created, and the initial coordinates of residues are initialized. We initialize the initial coordinates of all residues randomly on the surface of a sphere of sufficiently small radius. When generating initial configurations, a fixed seed is also used for reproducibility. Within a single residue sequence, the initial coordinates of residues are chosen to be the same. This is done to reduce the probability of the system converging to macrostates that differ significantly in their spatial distribution.

Stage 3. Achievement of thermal equilibrium for each replica. At this stage, the Monte Carlo method with the Metropolis algorithm is used. At each step of the algorithm, a new configuration  $R' = R + \delta R$  is proposed, where  $\delta R$  is a random displacement with a Gaussian distribution. The displacement amplitude is controlled and adapted individually for each replica. If the acceptance rate for a given replica falls below the target value (by default, this value is 0.3), the step size is decreased; if it is higher, the step size is increased. Such individual adaptation allows each replica to efficiently explore its region of phase space independently of others. To prevent the system from getting stuck in local minima, simulated annealing is used. The procedure starts with a low value of inverse temperature  $\beta = \frac{1}{k_B T}$  (which corresponds to a high temperature  $T$ ) and gradually increases  $\beta$  to the target value according to a linear law:  $\beta_{\text{current}} = \beta_{\text{initial}} + (\beta_{\text{final}} - \beta_{\text{initial}}) \cdot \frac{\text{step}}{\text{total\_steps}}$ . The energy change  $\Delta E = E(R', \sigma) - E(R, \sigma)$  is computed using formula (1), including all energy contributions. The transition to the new state is accepted with probability  $P_{\text{accept}} = \min(1, \exp(-\beta \Delta E))$ . The procedure is repeated for  $N_{\text{eq}}$  steps until thermal equilibrium is reached. The criterion for equilibrium is stabilization of the average energy.

Stage 4. Collection of statistically independent configurations for each replica. At this stage, after reaching equilibrium,  $N_{\text{prod}}$  Monte Carlo steps are performed, during which the current configuration is saved every  $\tau$  steps. The parameter  $\tau$  is chosen to be larger than the correlation time of the system, which guarantees the statistical independence of the saved configurations. As a result, for each replica, a set of  $S = \frac{N_{\text{prod}}}{\tau}$  configurations  $\{R^{(k,m,s)}\}_{s=1}^S$  is obtained, representing a sample from the canonical distribution. These configurations characterize the macrostate (replica) as a statistical ensemble.

Stage 5. Computation of the overlap matrix between replicas. At this stage, for each sequence  $k$  independently, the overlap matrix  $q_{mn}^{(k)}$  of dimension  $M \times M$  is computed according to definition (5). Next, for each sequence  $k$ , the distance matrix  $D_{mn}^{(k)} = 1 - q_{mn}^{(k)}$  is determined. At this stage, a key difference of our approach from the standard analysis of disordered heteropolymers is realized. The overlap matrix  $q_{mn}^{(k)}$  and, consequently, the distance matrix  $D_{mn}^{(k)}$  are computed for each sequence  $k$  independently. No averaging of these matrices over the ensemble of sequences (i.e., over the disorder index  $k$ ) is performed. All subsequent steps of analysis (selection of unique replicas, verification of ultrametricity) are also performed individually for each disorder realization. Additionally, at this stage, the Edwards–Anderson parameter  $q_{\text{EA}}^{(k)}$  is computed as the average of the off-diagonal elements of the overlap matrix:

$$q_{\text{EA}}^{(k)} = \frac{2}{M(M-1)} \sum_{m < n} q_{mn}^{(k)},$$

which serves as an indicator of the spin glass phase.

Stage 6. Verification of ultrametricity for each sequence. Before analyzing the ultrametric structure, it is necessary to ensure that the considered replicas indeed represent different macrostates. In non-ergodic systems, such as spin glasses and proteins, different initial microstates may converge to the same macrostate (replica). If the system is non-ergodic, then there exist many different macrostates. Upon random initialization, some replicas may fall into the basin of attraction of the same macrostate, leading to overlap values close to unity. To correctly identify hierarchical organization, it is necessary to exclude such "duplicate" replicas and perform the analysis only on the set of replicas corresponding to different macrostates. In the proposed algorithm, we introduce a procedure for selecting unique replicas based on the overlap matrix. For a fixed sequence  $k$ , all pairs of replicas  $(m, n)$  are considered. If the condition  $q_{mn}^{(k)} > 1 - \varepsilon_{\text{rep}}$  is satisfied, where  $\varepsilon_{\text{rep}}$  is a user-defined threshold (in this work,  $\varepsilon_{\text{rep}} = 0.2$  is adopted), then such replicas are considered to belong to the same macrostate. From each group of equivalent replicas, only one is retained; the others are excluded from further consideration. As a result, for sequence  $k$ , a reduced set of  $M'_k \leq M$  unique replicas is formed. The corresponding distance matrix  $D^{(k)}$  is truncated to dimension  $M'_k \times M'_k$ .

After selecting unique replicas, the distance matrix  $D^{(k)}$  is analyzed according to the following algorithm. For each sequence  $k$ , all triangles formed by triples of replicas  $(i, j, l)$  from  $M'_k$  are considered. For each triangle, the three distances  $D_{ij}, D_{il}, D_{jl}$  are computed and ordered in increasing order:  $D_{\min} \leq D_{\text{mid}} \leq D_{\max}$ . Then, using given accuracy parameters  $\epsilon$  and  $\delta$  with  $\delta > \epsilon$ , the triangle is classified as follows:

1. If  $\frac{D_{\max} - D_{\min}}{D_{\min}} < \epsilon$ , the triangle is considered trivially ultrametric.

2. If  $\frac{D_{\max} - D_{\text{mid}}}{D_{\text{mid}}} < \epsilon$  and  $\frac{D_{\text{mid}} - D_{\min}}{D_{\text{mid}}} \geq \delta$ , the triangle is considered nontrivially ultrametric.

3. Otherwise, the triangle is classified as non-ultrametric.

Next, for each sequence  $k$ , the fraction of trivially ultrametric triangles  $f_{\text{triv}}^{(k)}$ , the fraction of nontrivially ultrametric triangles  $f_{\text{nontriv}}^{(k)}$ , the total fraction of ultrametric triangles  $f_{\text{ultra}}^{(k)} = f_{\text{triv}}^{(k)} + f_{\text{nontriv}}^{(k)}$ , and the fraction of non-ultrametric triangles  $f_{\text{non}}^{(k)} = 1 - f_{\text{ultra}}^{(k)}$  are computed. A sequence is considered to demonstrate ultrametricity if  $f_{\text{ultra}}^{(k)} > 0.5$ . In this case, if  $f_{\text{nontriv}}^{(k)} > f_{\text{triv}}^{(k)}$ , the ultrametricity is classified as nontrivial; otherwise, it is classified as trivial.

Stage 7. Classification of ultrametricity type and aggregation of results. At this stage, based on the classification of individual sequences, summary statistics over the ensemble are formed. Specifically, the total number and fraction of sequences for which ultrametricity was detected, the number and fraction of sequences with predominance of nontrivial and trivial ultrametricity, and the average fractions of trivial, nontrivial, total ultrametric, and non-ultrametric triangles, as well as their standard deviations, are determined.

Stage 8. Repeated simulation. After completing Stage 7, those sequences for which nontrivial ultrametricity was detected are selected. Then, for the selected sequences, a repeated simulation (Stages 1–7) is performed with the same model and simulation parameters but with a changed random number generator seed. This ensures independence of thermal fluctuations and initial conditions from the first stage.

The described algorithm completely excludes the operation of averaging overlap matrices over the ensemble of sequences. Each sequence is considered as an independent disorder realization with its own unique energy landscape. This allows correctly estimating what fraction of sequences demonstrate nontrivial ultrametricity and identifying sequence parameters favorable for the formation of hierarchical structure.

## 4 Simulation results

This section presents the results of a computational experiment conducted in accordance with the algorithm described above. The simulation was performed on an NVIDIA Tesla P100 graphics processor using a developed program in the Python language with the PyTorch library. Below are the main parameters of the model and simulation, justification for the choice of initialization method, detailed numerical results of the first and second stages, and their analysis.

The simulation parameters in the numerical experiment were chosen as follows. The chain length is  $N = 128$  residues, the number of independent disorder realizations (number of sequences) is  $K = 50$ , the number of replicas for each sequence is  $M = 50$ , the inverse temperature is  $\beta = 1.0$  (temperature  $T = 1.0$  in units of  $k_B = 1$ ). To improve convergence, simulated annealing was used with an initial temperature  $T_{\text{initial}} = 10.0$ . The number of steps to reach equilibrium was  $n_{\text{equil}} = 100\,000$ , the number of production steps at the statistics collection stage was  $n_{\text{prod}} = 40\,000$ , the configuration saving interval was  $\tau = 100$  (thus, each replica is represented by  $S = 400$  independent configurations). The initial step size in the Metropolis algorithm was chosen as 0.15 with individual adaptation for each replica to maintain an acceptance rate around 0.3. Ultrametricity verification parameters:

$\varepsilon = 0.05$ ,  $\delta = 0.1$ , threshold for identical replicas  $\varepsilon_{rep} = 0.2$ . Probabilities of residue types:  $p_{hp} = 0.4$  (hydrophobic),  $p_+ = 0.25$  (positively charged),  $p_- = 0.25$  (negatively charged),  $p_{neut} = 0.1$  (neutral). Potential parameters:  $\sigma_{rep} = 1.0$ ,  $\varepsilon_{rep} = 1.0$  (repulsion);  $\sigma_{LJ} = 1.0$ ,  $\varepsilon_{LJ} = 5.0$ ,  $r_{cut} = 4.0$  (Lennard–Jones);  $r_{bond} = 1.0$ ,  $k_{bond} = 10.0$  (elastic bonds);  $k_{coul} = 1.0$ ,  $\lambda_{Debye} = 2.0$ ,  $r_{min} = 0.5$  (Coulomb interaction with screening).

It is important to note that the choice of specific values for the accuracy parameters  $\varepsilon = 0.05$  and  $\delta = 0.1$  is purely heuristic. These values were determined empirically. They provide a reasonable balance between the strictness of the ultrametricity criterion and the sensitivity of the method to the presence of hierarchical structure, given the inevitable statistical fluctuations inherent in computational experiments. Too small values of  $\varepsilon$  and  $\delta$  would lead to the vast majority of triangles being classified as non-ultrametric due to statistical noise, even in the presence of clear hierarchical organization. Too large values, on the contrary, could classify as ultrametric triangles that do not satisfy the strict triangle inequality. The chosen values, based on preliminary test calculations, allowed achieving this balance and, as will be shown below, revealed a clear picture of the predominance of nontrivial ultrametricity. Nevertheless, the question of the influence of the values of  $\varepsilon$  and  $\delta$  on the final results and the search for their optimal values remains a subject of separate investigation.

A remark should also be made regarding the choice of interaction potential parameters listed above. These parameters are not universal and were not extracted from any experimental data, which is in principle impossible for such a coarse model. On the contrary, they were selected during preliminary computational experiments with the aim of creating conditions in which the ultrametric properties of the energy landscape could manifest most clearly. In other words, we purposefully attempted to find parameter values at which the system demonstrates a sufficiently high level of frustration (to avoid trivial behavior) and retains the ability to form a hierarchical structure of states. The criterion for such selection was the maximization of the fraction of sequences with nontrivial ultrametricity in several test runs. It is also important to emphasize that a complete scan of the multidimensional parameter space (interaction energies, screening length, bond stiffness, etc.) is an extremely resource-intensive task, beyond the scope of this study. Therefore, the values presented in the work, although allowing successful verification of the presence of ultrametricity in the model, nevertheless do not claim to be optimal or unique.

When conducting the simulation, we used initialization of the initial coordinates of all residues randomly on the surface of a sphere of small radius (in this experiment, the sphere radius was taken as 1.0 in arbitrary units). This choice is motivated by the following considerations. First, starting from a compact configuration (in which all residues are concentrated near the origin) avoids situations where the chain is completely extended and the folding process would require excessively long times to reach equilibrium globular states. Second, we deliberately exclude from consideration macrostates corresponding to distributions in the subspace of extended configurations, since they are certainly not related to the region of phase space of interest to us, associated with compact structures. Furthermore, within a single sequence, we set the same initial coordinates for all replicas. This was done to reduce the probability that different replicas would initially find themselves in significantly different regions of configuration space. With the same start, all replicas have equal chances to converge to the same or different macrostates, but the influence of randomness of initial conditions is minimized. This approach allows more clearly identifying effects associated

precisely with the shape of the energy landscape, rather than with trivial scatter of initial configurations.

In the first stage, all 50 sequences were processed. The key results can be summarized as follows. All 50 replicas in each of the 50 sequences were found to be unique. Of the 50 sequences, ultrametricity (i.e., fraction of ultrametric triangles  $f_{ultra}^{(k)} > 0.5$ ) was detected in 45 sequences, which constitutes 90.0% of the total. Among the sequences demonstrating ultrametricity, in the vast majority (44 out of 45, i.e., in 97.8% of cases), nontrivial ultrametricity predominates, meaning the fraction of triangles satisfying the conditions of isoscelesness with a clear distinction between the small and medium distances exceeds the fraction of trivially equilateral triangles. Only in one sequence was predominance of trivial ultrametricity observed. The average fractions of triangles over the ensemble of sequences were: trivial  $19.31\% \pm 9.26\%$ , nontrivial  $46.07\% \pm 5.24\%$ , total ultrametricity  $65.38\% \pm 12.48\%$ . The high standard deviation for the trivial and total fractions indicates significant variability of landscapes from sequence to sequence. The Edwards–Anderson parameter, averaged over the ensemble of sequences, was  $\langle q_{EA} \rangle = 0.292 \pm 0.066$ . This value is noticeably above zero and indicates that the system is near the glass transition temperature, where ergodicity is broken and many different macrostates exist. The range of  $q_{EA}$  lies between 0.156 and 0.433, confirming that even within a single model, different sequences can lead to different degrees of "glassiness." The average maximum distance between residues in the collected configurations was about 7.14 in arbitrary units, which corresponds to a compact globular structure (for comparison, a completely extended chain of length 128 with step 1 would have a length on the order of 127). Based on the results of the first stage, all 44 sequences in which nontrivial ultrametricity was detected were selected for the second stage.

The second stage was performed for the selected 44 sequences with a changed random number generator seed, which ensured independence of the Monte Carlo trajectories from the first stage. All other model and simulation parameters remained unchanged. Of the 44 sequences, ultrametricity was confirmed for 42 sequences (95.5%). Two sequences no longer satisfied the criterion  $f_{ultra} > 0.5$ . In 41 out of 42 cases (97.7%), nontrivial ultrametricity again predominated. The average fractions of triangles over the ensemble of the second stage were: trivial  $19.93\% \pm 8.86\%$ , nontrivial  $47.67\% \pm 3.03\%$ , total ultrametricity  $67.59\% \pm 9.23\%$ . These values are close to those obtained in the first stage, indicating the statistical stability of the observed patterns. The average value of  $q_{EA}$  was  $0.284 \pm 0.055$ , practically coinciding with the first stage. The average maximum distance also remained practically at the previous level — 7.11. The fact that two sequences out of 44 no longer met the ultrametricity criterion upon repeated simulation can be explained by two main reasons. First, the change in initial initialization and subsequent annealing could have led to the set of achieved macrostates for this sequence being different. As a result, among the replicas, those replicas that formed the ultrametric subset could be absent, or the subset of replicas itself could have changed. Second, during the Monte Carlo dynamics associated with collecting statistically independent configurations, some replicas could over time, with some (though not very large) probability, change their basin of attraction and end up in a different valley, which could lead to distortion of the collected statistical data. The reason for this is that although we use adaptive step size and simulated annealing, it is impossible to completely exclude transitions between macrostates in a finite simulation, especially if the energy barriers are not too high. Thus, the observed "disappearance" of ultrametricity for some sequences does not contradict the

overall picture but rather emphasizes the sensitivity of the hierarchical structure to the specific set of replicas generated by stochastic dynamics.

The simulation results are presented in Figures 1–3.

Figure 1 shows the distributions of fractions of ultrametric triangles over the ensemble of 50 random sequences at the first stage. Columns outlined with solid lines without fill show the distribution of the total fraction of all ultrametric triangles  $f_{\text{ultra}}$ , and columns with gray fill outlined with dashed lines show the distribution of the fraction of nontrivial ultrametric triangles  $f_{\text{nontriv}}$ . Both distributions have distinct maxima: for  $f_{\text{ultra}}$  in the region 0.65–0.75, for  $f_{\text{nontriv}}$  in the region 0.45–0.50. The asymmetry of the  $f_{\text{nontriv}}$  distribution with a gentler left slope indicates that a significant portion of sequences have moderate values of nontrivial ultrametricity. Note that  $f_{\text{ultra}} = f_{\text{triv}} + f_{\text{nontriv}}$ , and from the first stage data for the averages we have  $\langle f_{\text{ultra}} \rangle \sim 68\%$ ,  $\langle f_{\text{nontriv}} \rangle \sim 48\%$ ,  $\langle f_{\text{triv}} \rangle \sim 20\%$ . Thus, the contribution of the trivial component is not dominant but is also not negligible. The fact that a significant part of sequences have  $f_{\text{nontriv}} \sim 0.5$  should not cause surprise. Nontrivial ultrametricity is a stricter criterion of hierarchical organization than total ultrametricity. In real systems with finite fluctuations, there will always be some number of "borderline" triangles that are classified as trivially ultrametric. In this case, in the vast majority of ultrametric sequences, predominance of the nontrivial component is observed ( $f_{\text{nontriv}} > f_{\text{triv}}$ ).

Figure 2 presents a graph of the correlation between the Edwards–Anderson parameter  $q_{\text{EA}}$  and the fraction of nontrivial ultrametric triangles  $f_{\text{nontriv}}$  for 50 sequences at the first stage. Filled black circles denote sequences for which the total fraction of ultrametric triangles exceeds 0.5 (ultrametric), empty squares denote the remaining (non-ultrametric) sequences. A non-monotonic structure of the point distribution is clearly observed, with a maximum in the region  $q_{\text{EA}} \approx 0.2 - 0.30$ , where  $f_{\text{nontriv}}$  reaches values  $\sim 0.50$ . This indicates the existence of an optimal level of frustration at which the hierarchical organization of the energy landscape is most pronounced. At lower values of  $q_{\text{EA}}$ , the system is insufficiently frustrated to form a developed hierarchy, while at high  $q_{\text{EA}}$  ( $> 0.35$ ), excessive frustration leads to "blurring" of boundaries between macrostates and suppression of ultrametricity. Sequences not satisfying the ultrametricity criterion are concentrated predominantly in the region of high  $q_{\text{EA}} > 0.35$ , confirming the connection between strong frustration and loss of hierarchical structure.

Figure 3 shows a dendrogram of hierarchical clustering of 50 replicas for the sequence with the maximum fraction of nontrivial ultrametric triangles at the second stage (sequence with  $f_{\text{nontriv}} = 51.02\%$ ,  $f_{\text{ultra}} = 76.37\%$ ). The distance matrix is defined as  $D = 1 - q$ , where  $q$  is the overlap between replicas. The average linkage method was used in constructing the dendrogram. Characteristic asymmetry is clearly visible on the graph: the merging levels of clusters in the left part of the dendrogram are significantly higher than in the right part. High merging levels in the left part ( $D \sim 0.75 \div 0.95$ ) correspond to the merging of large clusters of macrostates separated by significant energy barriers. These clusters represent fundamentally different conformational families (e.g., chain folds with different spatial architectures). Transition between such families requires overcoming high barriers and is kinetically forbidden under low-temperature conditions, which is reflected in the large distance between the corresponding replicas. In the right part of the dendrogram, merging levels are located significantly lower ( $D \approx 0.3 - 0.5$ ). This indicates the existence of a hierarchy of substates within large clusters. Replicas are grouped into compact groups at

small distances, then these groups merge at intermediate distances, and only then merging with other large clusters occurs at high levels. It is important to note that such asymmetry (high levels on the left, low on the right) is not an artifact of a specific sequence but reflects a general property of ultrametric spaces: the existence of a distinguished "root" of the hierarchy and many "leaves" grouping at different levels. In terms of spin glass theory, this corresponds to the structure of the Parisi tree, where pure states are organized into a hierarchy with different scales of overlaps. The observed dendrogram demonstrates that even in our simplified protein prototype model, the space of macrostates exhibits a similar structure.

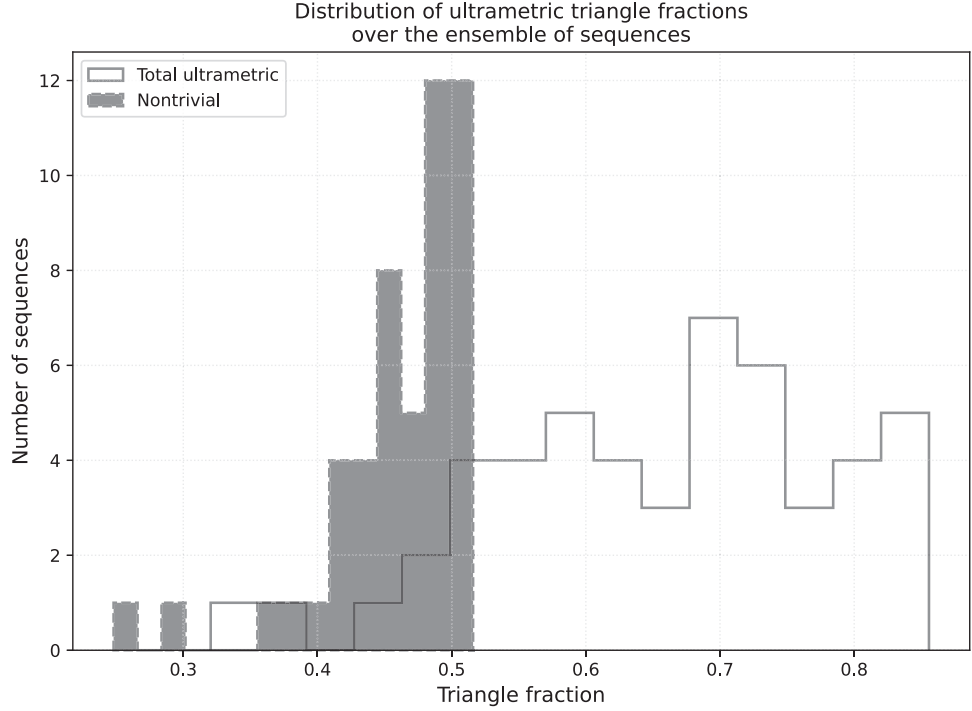


Figure 1: Histogram of the distribution of fractions of ultrametric triangles over the ensemble of 50 random sequences (first stage). Columns outlined with a solid line show the distribution for the total fraction of ultrametric triangles  $f_{\text{ultra}}$ . Columns outlined with a dashed line with gray fill show the distribution for the fraction of nontrivial ultrametric triangles  $f_{\text{nontriv}}$ . The peak of the  $f_{\text{nontriv}}$  distribution occurs in the region  $0.45 - 0.50$ , indicating the predominance of nontrivial hierarchical organization.

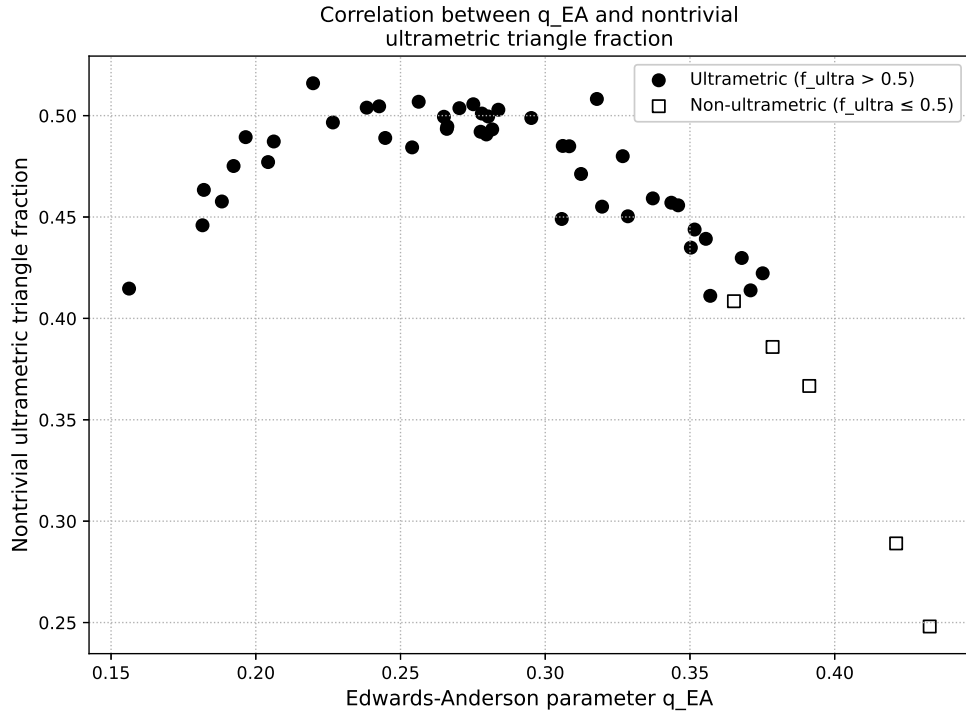


Figure 2: Correlation between the Edwards–Anderson parameter  $q_{EA}$  and the fraction of nontrivial ultrametric triangles  $f_{\text{nontriv}}$  for 50 sequences (first stage). Filled black circles denote sequences for which the total fraction of ultrametric triangles exceeds 0.5 (ultrametric), empty squares denote the remaining (non-ultrametric) ones. A non-monotonic structure is observed: maximum values of  $f_{\text{nontriv}}$  are achieved at  $q_{EA} \approx 0.25 - 0.30$ , indicating the existence of an optimal level of frustration for the formation of a hierarchical landscape. At higher values of  $q_{EA}$  ( $>0.35$ ), ultrametricity is typically not detected.

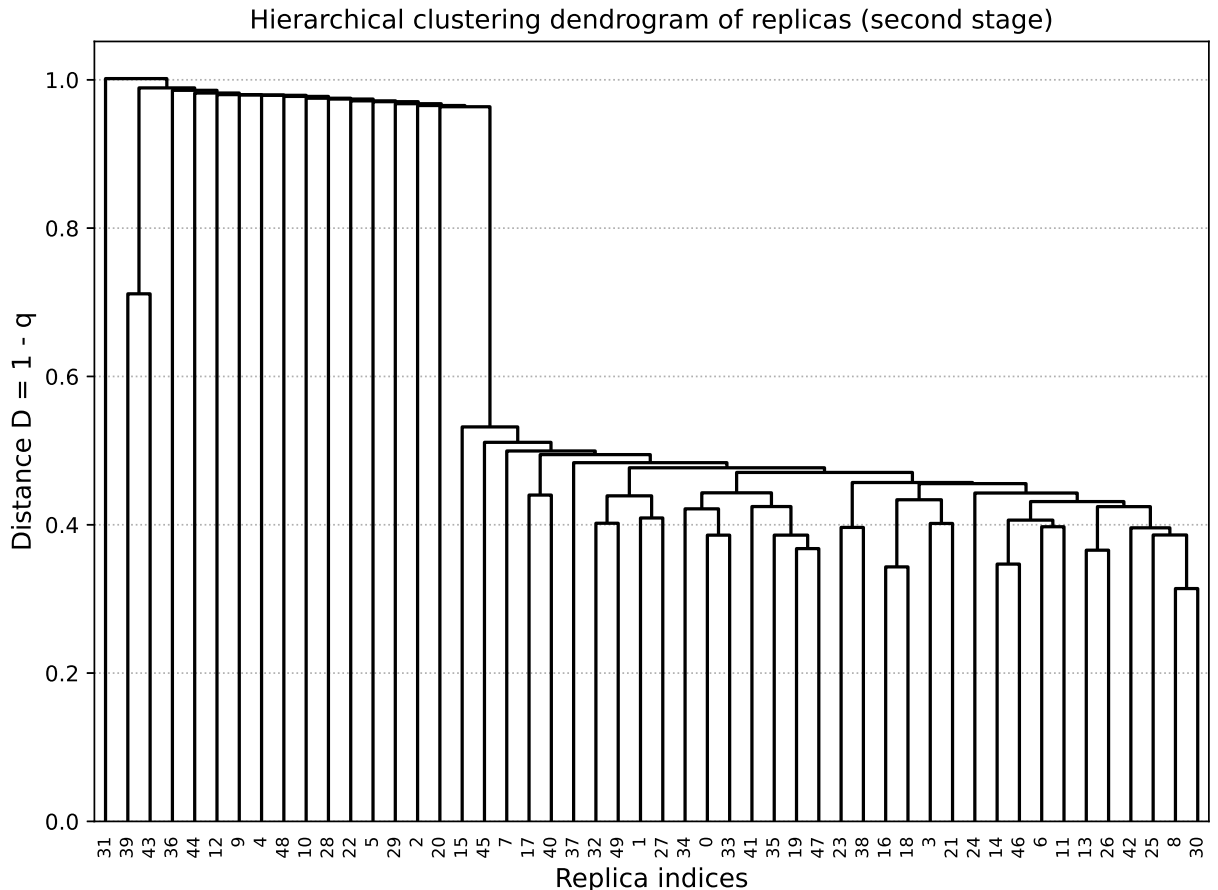


Figure 3: Dendrogram of hierarchical clustering of 50 replicas for the sequence with the maximum fraction of nontrivial ultrametric triangles at the second stage (sequence with  $f_{\text{nontriv}} = 51.02\%$ ,  $f_{\text{ultra}} = 76.37\%$ ). The distance matrix is defined as  $D = 1 - q$ , where  $q$  is the overlap between replicas. The average linkage method was used in constructing the dendrogram. An asymmetric structure is clearly visible: in the left part of the dendrogram, the merging levels of clusters ( $D \sim 0.7 - 0.9$ ) are significantly higher than in the right part ( $D \sim 0.3 - 0.5$ ). This corresponds to a hierarchy of macrostates: large clusters separated by high barriers (left part) contain internal subclusters corresponding to closer substates (right part). Such a structure is a characteristic feature of ultrametric organization of state space.

Analysis of the obtained results allows drawing several important conclusions. First of all, even in such a simplified model, where the protein is represented only by a chain of point particles with a limited set of interactions and with heuristic selection of potential parameters and classification thresholds, the energy landscape exhibits clear signs of ultrametric organization. This is manifested in the fact that, according to the results of two stages, for the vast majority of random sequences (80%), the distance matrix between replicas contains more than 50% of triangles satisfying the ultrametric inequality, in which the nontrivial type of ultrametricity predominates. This points to a real hierarchical structure, rather than an artifact of equilateral triangles that could arise, for example, from random scatter of points in a high-dimensional space. It is important to emphasize that ultrametricity is not required

to manifest in all sequences without exception. The structure of the energy landscape is determined by the specific set of interactions encoded by the amino acid sequence. In some disorder realizations, frustrations may be weak, and the system may behave more like a simple glass without a pronounced hierarchy, or like a system with a single macrostate. Our results show that about 20% of sequences do not yield a sufficient fraction of ultrametric triangles ( $f_{ultra} \leq 0.5$ ). This is natural and expected. Moreover, even within a single sequence possessing an ultrametric landscape, not all possible triples of replicas are required to be ultrametric. Ultrametricity is a property that may hold for some subset of states corresponding, for example, to those macrostates responsible for globular structures with a certain architecture. In our simulation, we observe that the fraction of ultrametric triangles ranges from 40% to 87%, indicating that the hierarchy covers a significant, but not necessarily all, set of macrostates.

Thus, the totality of obtained data — the high fraction of nontrivially ultrametric sequences, the stability of this property upon repeated simulation, the presence of an optimal level of frustration, and the characteristic asymmetry of dendrograms — indicates that the heuristically chosen potential parameters and classification thresholds indeed allowed revealing a property intrinsic to the model: hierarchical organization.

## 5 Conclusion and perspectives

In this work, we have presented and implemented a computational scheme for testing the ultrametricity of the energy landscape in a simple model of a protein prototype, where amino acid residues are modeled as material points, and pairwise interactions include universal repulsion, the Lennard-Jones potential for hydrophobic residues, Coulomb interaction with screening for charged residues, and elastic bonds between neighbors. A key feature of this scheme is the definition of macroscopic overlap between replicas through the correlation of vectors of mean pairwise energies, which is completely analogous to the approach in spin glass theory and allows applying the statistical apparatus of replica theory. It is important to emphasize that, in contrast to the classical approach in the theory of disordered heteropolymers, in this work we fundamentally refrain from the procedure of averaging over disorder. The analysis is performed for each specific residue sequence independently, which corresponds to the uniqueness of each molecule and allows revealing the connection between a specific disorder realization and the structure of its energy landscape. The computational algorithm includes stages of generating an ensemble of random sequences, achieving equilibrium with simulated annealing and adaptive Monte Carlo step size, collecting statistically independent configurations, computing overlap matrices, and analyzing ultrametricity with discrimination between trivial and nontrivial types.

Numerical modeling was performed for a system with chain length  $N = 128$ , number of sequences  $K = 50$ , number of replicas  $M = 50$ , and sample size  $S = 400$  for each replica. The results obtained indicate that even in an extremely simplified model, the energy landscape exhibits pronounced signs of ultrametric organization. In the vast majority of random sequences, a high fraction of ultrametric triangles was recorded in the distance matrix between replicas, with the dominant contribution coming from the nontrivial component. This points to the presence of a hierarchical structure, rather than an artifact of equilateral trian-

gles characteristic of trivial ultrametricity. The values of the Edwards–Anderson parameter confirm that the system is near the spin glass phase with broken ergodicity. A repeated experiment for selected sequences demonstrated the statistical stability of the observations, although a small fraction of systems lost their ultrametric property, which is explained by the stochastic nature of the Monte Carlo method and possible mixing of replicas between macrostates. Correlation analysis revealed a non-monotonic dependence between the degree of frustration and the level of ultrametricity, indicating the existence of an optimal level of disorder favorable for the formation of a hierarchical landscape. Dendrograms for sequences with maximal ultrametricity clearly demonstrate an asymmetric structure: large clusters corresponding to fundamentally different conformational families are separated by large distances, while within them a finer hierarchy of substates is observed. These results provide additional numerical arguments in favor of Frauenfelder’s hypothesis about the hierarchy of conformational substates of proteins [19, 20, 21] and show that ultrametricity may be an intrinsic property of even very coarse models that imitate only the most general features of polypeptide chains. The high fraction of sequences with nontrivial ultrametricity, obtained in the absence of any angular interactions or specific orientational effects, suggests that hierarchical organization is a fundamental consequence of the competition between long-range and short-range forces in a polymer chain with disorder.

In our opinion, further research in this direction should be aimed at a systematic study of how the complication of the model affects the ultrametric properties of the energy landscape. To this end, one should sequentially introduce new elements into the model, starting from the simplest and gradually moving to more complex descriptions. At each stage, it is necessary to verify whether ultrametricity is preserved and how its quantitative characteristics change. Such an approach will allow identifying the minimal set of physical interactions necessary for the formation of hierarchical structure.

First of all, the dependence of ultrametricity on temperature should be studied. It is expected that with decreasing temperature, the degree of ultrametricity will increase, reaching saturation in the spin glass phase, whereas at high temperatures the landscape should become simpler, more ergodic, which should lead to a decrease in the fraction of nontrivial ultrametric triangles. Such behavior is predicted by spin glass theory and has been observed in numerical experiments for the Edwards–Anderson model [12, 13, 15]. It is important to quantitatively characterize this transition by determining the glass transition temperature  $T_g$  for this model through the temperature dependence of the Edwards–Anderson parameter. Next, the dependence of the degree of ultrametricity on system size  $N$  should be investigated, since with increasing chain length, the number of degrees of freedom increases, and one can expect a complication of the hierarchical structure. Also important is the systematic variation of sequence composition (probabilities of occurrence of hydrophobic, charged, and neutral residues). This will allow constructing a phase diagram in composition space and identifying regions where ultrametricity is most pronounced.

Despite the obtained evidence in favor of ultrametricity, it is necessary to be aware of the limitations of the model. These limitations may affect the generality of our conclusions and must be overcome when moving towards more realistic descriptions. The main simplification is the representation of amino acid residues as material points devoid of spatial structure. In reality, each residue has volume, shape, and a specific orientation in space, which is critically important for the specificity of interactions. Neglecting these factors means that

we completely ignore steric effects (related to side chain packing) and the possibilities of forming directed interactions, such as hydrogen bonds and ionic pair potentials, which require a specific mutual orientation of partners. Furthermore, our model lacks any angular degrees of freedom: a real polypeptide chain possesses rigidity associated with valence and torsion angles, which leads to the formation of secondary structure elements — alpha helices and beta sheets. These structures are not only stabilized by hydrogen bonds but also impose strong constraints on the configuration space, potentially creating additional levels of hierarchy. The absence of explicit solvent modeling also limits the realism of the model: hydrophobic attraction is accounted for only through an effective pairwise Lennard-Jones potential, which does not capture the collective nature of the hydrophobic effect, and also completely ignores medium viscosity and hydration dynamics. In addition, the potentials used in the model are extremely coarse: the Lennard-Jones potential with uniform parameters for all hydrophobic residues does not reflect differences between, for example, aliphatic and aromatic side chains, and Coulomb interaction with constant screening does not account for the inhomogeneity of the dielectric constant inside the protein and near its surface.

The enumerated limitations naturally indicate ways to extend the model, which will bring it closer to real proteins and allow testing the stability of ultrametric properties under more realistic conditions. The first and most conceptually important step is to abandon the point particle approximation and introduce the spatial structure of residues. In the original model, each residue is represented by a single point in three-dimensional space. The generalization consists in modeling each residue  $i$  by a set of  $L$  interacting centers (sites)  $\{r_{i,1}, r_{i,2}, \dots, r_{i,L}\}$ , where  $r_{i,\alpha} \in \mathbb{R}^3$  are the coordinates of the  $\alpha$ -th site of residue  $i$ . These sites are rigidly connected to each other, meaning their mutual arrangement is fixed and determines the shape of the residue. The state of residue  $i$  as a rigid body is completely described by six degrees of freedom. To specify them, we choose some center in the residue (e.g., the center of mass or the position of the  $C_\alpha$  atom) with coordinates  $R_i \in \mathbb{R}^3$ . We specify the orientation of the residue by a right-handed triple of orthonormal vectors  $u_i, v_i, w_i \in \mathbb{R}^3$ . These vectors define the orientation of the local coordinate system associated with the residue relative to the laboratory system. The internal geometry of the residue is determined by the residue type, which we denote by  $\tau$ . For each type  $\tau$ , the coordinates of all its sites in the local coordinate system are given. Denote for a residue of type  $\tau$  the coordinates of its  $\alpha$ -th site as a vector:

$$a_{\tau,\alpha} = (a_{\tau,\alpha}^x, a_{\tau,\alpha}^y, a_{\tau,\alpha}^z) \in \mathbb{R}^3,$$

where  $\alpha = 1, \dots, L_\tau$ , and  $L_\tau$  is the number of sites for residues of this type. Each vector  $a_{\tau,\alpha}$  is a model parameter and does not change during the evolution of the system. The coordinates of the  $\alpha$ -th site of residue  $i$  (of type  $\tau_i$ ) in the laboratory coordinate system are expressed through the dynamic variables  $R_i, u_i, v_i, w_i$  and model parameters  $a_{\tau_i,\alpha}$  as follows:

$$r_{i,\alpha} = R_i + a_{\tau_i,\alpha}^x u_i + a_{\tau_i,\alpha}^y v_i + a_{\tau_i,\alpha}^z w_i. \quad (6)$$

The interaction energy between two residues  $i$  and  $j$  (of types  $\tau_i$  and  $\tau_j$ , respectively) equals the sum of pairwise interactions between all their sites:

$$U_{ij}(R_i, u_i, v_i, w_i, R_j, u_j, v_j, w_j) = \sum_{\alpha=1}^{L_{\tau_i}} \sum_{\beta=1}^{L_{\tau_j}} U_{\alpha\beta}(r_{i,\alpha}, r_{j,\beta}), \quad (2)$$

where  $r_{i,\alpha}$  and  $r_{j,\beta}$  are computed by formula (6), and  $U_{\alpha\beta}$  is the interaction potential between sites  $\alpha$  and  $\beta$ . It is important to emphasize that the potential  $U_{\alpha\beta}$  depends only on the coordinates of the sites. The dependence on orientation arises automatically, since the site coordinates, being arguments of  $U_{\alpha\beta}$ , themselves depend on orientation through formula (6).

In the simplest case, the interaction between sites may depend only on the distance between them. Then

$$U_{\alpha\beta}(r_{i,\alpha}, r_{j,\beta}) = U_{\alpha\beta}(|r_{i,\alpha} - r_{j,\beta}|).$$

To model attraction between specific types of sites, one can use the Lennard-Jones potential of the form (2). For charged sites, one can add Coulomb interaction with screening of the form (3). To account for more subtle effects related to the mutual orientation of sites (for example, if the sites represent planar groups), the potential may depend not only on distance but also on direction. In this case, potentials can be used whose arguments include vectors constructed from site coordinates. For example, if site  $\alpha$  has a distinguished direction given by a unit vector  $n_{i,\alpha}$ , which is also rigidly connected to the residue and computed through  $u_i, v_i, w_i$  similarly to coordinates, then one can define a potential of the form:

$$U_{\text{orient}}(r_{i,\alpha}, r_{j,\beta}, n_{i,\alpha}, n_{j,\beta}) = \varepsilon_{\text{orient}} \left[ \left( \frac{\sigma_{\text{orient}}}{|r_{i,\alpha} - r_{j,\beta}|} \right)^{12} - \left( \frac{\sigma_{\text{orient}}}{|r_{i,\alpha} - r_{j,\beta}|} \right)^6 \right] \cdot f(n_{i,\alpha}, n_{j,\beta}, r_{i,\alpha} - r_{j,\beta}),$$

where the function  $f$  depends on scalar products of the type  $n_{i,\alpha} \cdot n_{j,\beta}$  and  $n_{i,\alpha} \cdot (r_{i,\alpha} - r_{j,\beta})$ . Such a functional form allows modeling preferred mutual orientations without reference to specific chemistry.

Potentials defining chain geometry can be implemented as follows. In real polymer chains, neighboring monomers are connected by covalent bonds, which imposes constraints on the distances between them, as well as on the angles between bonds. To account for these constraints in the model, one can introduce potentials depending on the mutual arrangement of consecutive residues along the chain. If a distinguished center is defined for each residue  $i$  (e.g., the center of mass or the position of the  $C_\alpha$  atom) with coordinates  $R_i$ , then the distance between centers of neighboring residues  $|R_{i+1} - R_i|$  can be maintained near a fixed value using an elastic potential of the form (4). To describe valence angles formed by three consecutive residues, one can use a potential of the form

$$U_{\text{angle}}(\theta_i) = \frac{1}{2} k_\theta (\theta_i - \theta_0)^2, \quad (7)$$

where  $\theta_i$  is the angle between the vectors  $R_i - R_{i-1}$  and  $R_{i+1} - R_i$ , the parameter  $k_\theta > 0$  is the angular stiffness, and the parameter  $\theta_0$  is the equilibrium value of the valence angle. To describe torsion angles, which determine rotation around bonds, one can introduce a potential depending on the dihedral angle  $\phi_i$  formed by four residues  $i - 2, i - 1, i, i + 1$ :

$$U_{\text{dihedral}}(\phi_i) = \sum_{n=1}^N K_n [1 + \cos(n\phi_i - \delta_n)], \quad (8)$$

where  $K_n$  are amplitude parameters, and  $\delta_n$  are phase shift parameters. The choice of parameters for these potentials allows creating preferred chain conformations, for example, favoring helical or sheet structures.

The potential (7) is three-body, and the potential (8) is four-body. The introduction of many-body potentials requires a corresponding generalization of the replica comparison method. The vector  $\bar{u}^{(k,m)}$ , which we use to define overlap, can no longer be limited to only pairwise energies, since it would not contain information about many-body contributions that may be significant for the structure of the energy landscape. The most natural generalization consists in including all types of energies present in the model in this vector. Define for each replica  $m$  of sequence  $k$  a vector  $\bar{w}^{(k,m)}$ , whose components are: average values of pairwise energies  $\langle U_{ij} \rangle$  for all  $i < j$ ; average values of angular energies  $\langle U_{\text{angle}}(\theta_i) \rangle$  for all  $i$ ; average values of torsion energies  $\langle U_{\text{dihedral}}(\phi_i) \rangle$  for all  $i$ . The vector  $\bar{w}^{(k,m)}$  has dimension equal to the total number of all independent energy contributions in the model and contains all available information about the thermodynamic averages of the various energy components of the system. Then the overlap between replicas  $m$  and  $n$  for sequence  $k$  is defined as the Pearson correlation coefficient according to formula (5) with the substitution  $\bar{u}^{(k,m)} \rightarrow \bar{w}^{(k,m)}$ . With this approach, many-body interactions are naturally accounted for in the definition of overlap. This allows applying a unified methodology to models with arbitrary levels of complexity, from the simplest models with pairwise interactions to models with many-body potentials of any nature.

Also a natural generalization of the model is the introduction of a more detailed classification of residues, differing, for example, in size, shape, or nature of interaction. The original model uses only four types of residues, differing only in charge and hydrophobicity indicator. For a more refined study of the influence of sequence composition on ultrametricity, one can introduce a more detailed classification. Namely, each residue type  $\tau$  can be characterized by the following set of parameters: number of sites  $L_\tau$ , their relative coordinates  $\{a_{\tau,\alpha}\}_{\alpha=1}^{L_\tau}$ , site charges  $\{q_{\tau,\alpha}\}$ , Lennard-Jones potential parameters  $\{\varepsilon_{\text{LJ},\tau,\alpha\beta}, \sigma_{\text{LJ},\tau,\alpha\beta}\}$  for interaction between sites of different types, orientational interaction parameters, etc.

All the described extensions of the model can be introduced sequentially, which allows re-examining the ultrametric properties of the energy landscape at each stage. It is important to emphasize that the proposed analysis methodology — using macroscopic overlap based on vectors of mean energies and verifying the ultrametricity of the distance matrix — remains fully applicable at any level of model complexity. In the general case, the vector  $\bar{w}^{(k,m)}$  will include all types of energy contributions: pairwise, three-body, four-body, and so on. For each configuration, the corresponding values are computed, which are then averaged over the replica, after which the obtained vectors are used to calculate overlaps. This approach opens the possibility for a systematic study of the evolution of ultrametric properties as the model becomes more complex. The results obtained on the current, extremely simple model serve as a natural starting point for such an investigation. The observed picture suggests that the hierarchical structure of the landscape is embedded already at the most basic level of statistical description of a heteropolymer with competing interactions, and subsequent complication of the model merely builds upon this structure.

## References

- [1] G. Parisi, Infinite number of order parameters for spin-glasses, Phys. Rev. Lett. 43 (1979) 1754-1756. <https://doi.org/10.1103/PhysRevLett.43.1754> 1, 2

- [2] G. Parisi, A sequence of approximated solutions to the SK model for spin glasses, *Journal of Physics A: Mathematical and General* 13 (4) (1980) L115. <https://doi.org/10.1088/0305-4470/13/4/009> 1, 2
- [3] M. Mézard, G. Parisi, N. Surlas, G. Toulouse, M. Virasoro, Nature of the spin-glass phase. *Phys. Rev. Lett.* 52 (1984) 1156-1159. <https://doi.org/10.1103/PhysRevLett.52.1156> 1, 2
- [4] R. Rammal, G. Toulouse, M.A. Virasoro, Ultrametricity for physicists, *Rev. Mod. Phys.* 58(3) (1986) 765-788. <https://doi.org/10.1103/RevModPhys.58.765> 1
- [5] M. Talagrand, *Spin Glasses: A Challenge for Mathematicians*, Berlin: Springer, 2003. 1
- [6] M. Talagrand, Michel. The Parisi Formula, *Annals of Mathematics* 163 (1) (2006) 221–263. <http://www.jstor.org/stable/20159953> 1
- [7] M. Talagrand, *Mean Field Models for Spin Glasses*, Berlin: Springer, 2011. 1
- [8] D. Panchenko, The Parisi ultrametricity conjecture, *Annals of Mathematics* 177 (1) (2012) 383-393. <http://www.jstor.org/stable/23350562> 1
- [9] D. Panchenko, *The Sherrington-Kirkpatrick Model*, New York: Springer, 2013. 1
- [10] D. Panchenko, Structure of 1-RSB asymptotic Gibbs measures in the diluted  $p$ -spin models, *Journal of Statistical Physics* 162 (1) (2015) 1-22. <https://doi.org/10.1007/s10955-014-0955-5> 1
- [11] E. Subag, Free energy landscapes in spherical spin glasses, *Duke Mathematical Journal* 173 (7) (2024) 1291-1357. <https://doi.org/10.1215/00127094-2023-0033> 1
- [12] A.T. Ogielski, Dynamics of three-dimensional Ising spin glasses in thermal equilibrium, *Physical Review B* 32 (11) (1985) 7384-7398. <https://doi.org/10.1103/PhysRevB.32.7384> 1, 5
- [13] E. Marinari, G. Parisi, J. Ruiz-Lorenzo, F. Ritort, Numerical evidence for spontaneously broken replica symmetry in 3D spin glasses, *Physical review letters*, 76 (5) (1996) 843-846. <https://doi.org/10.1103/PhysRevLett.76.843> 1, 5
- [14] S. Franz F. Ricci-Tersenghi, Ultrametricity in three-dimensional Edwards-Anderson spin glasses. *Physical Review E* 61 (2) (2000) 1121-1124. DOI: <https://doi.org/10.1103/PhysRevE.61.1121> 1
- [15] P. Contucci, C. Giardinà, C. Giberti, C., G. Parisi, C. Vernia, Ultrametricity in the Edwards-Anderson model. *Physical Review Letters* 99 (5) (2007) 057206-057210. <https://doi.org/10.1103/PhysRevLett.99.057206> 1, 5
- [16] H.G. Katzgraber, A.P. Young, Probing the Almeida-Thouless line in spin glasses, *Physical Review B* 72 (18) (2006) 184416-1-184416-5. <https://doi.org/10.1103/PhysRevB.72.184416> 1

- [17] V. Martín-Mayor, J.J. Ruiz-Lorenzo, B. Seoane, A.P. Young, Numerical simulations and replica symmetry breaking. In *Spin Glass Theory and Far Beyond: Replica Symmetry Breaking After 40 Years* (2023) 69–93. [https://doi.org/10.1142/9789811273926\\_0005](https://doi.org/10.1142/9789811273926_0005) 1
- [18] N. Ghofraniha, J.G. Camara, S. Ferretti, S. Gentilini, D. Da Silva, C. Conti, Observation of ultrametricity in photonic spin glasses, *Research Square Preprint* (2025). <https://doi.org/10.21203/rs.3.rs-5433512/v1> 1
- [19] H. Frauenfelder, F. Parak, R.D. Young, Conformational substates in proteins, *Annual Review of Biophysics and Biophysical Chemistry* 17 (1) (1988) 451-479. <https://doi.org/10.1146/annurev.bb.17.060188.002315> 1, 5
- [20] H. Frauenfelder, S.G. Sligar, P.G. Wolynes, The energy landscapes and motions of proteins, *Science* 254 (5038) (1991) 1598-1603. <https://doi.org/10.1126/science.1749933> 1, 5
- [21] H. Frauenfelder, B.H. McMahon, Energy landscape and fluctuations in proteins, *Annalen der Physik* 8 (7-9) (1999) 655-667. <https://doi.org/10.1002/andp.200051209-1001> 1, 5
- [22] V.A. Avetisov, A.Kh. Bikulov, Protein ultrametricity and spectral diffusion in deeply frozen proteins, *Biophysical Reviews and Letters* 3 (3) (2008) 387-396. <https://doi.org/10.1142/S1793048008000836> 1
- [23] V.A. Avetisov, A.Kh. Bikulov, S.V. Kozyrev, Application of  $p$ -adic analysis to models of spontaneous breaking of replica symmetry, *Journal of Physics A: Mathematical and General* 32(50) (1999) 8785-8791. <https://doi.org/10.1088/0305-4470/32/50/301> 1
- [24] V.A. Avetisov, A.Kh. Bikulov, S.V. Kozyrev, V.A. Osipov,  $p$ -Adic Models of ultrametric diffusion constrained by hierarchical energy landscapes, *Journal of Physics A: Mathematical and General* 35(2) (2002) 177-189. <https://doi.org/10.1088/0305-4470/35/2/301> 1
- [25] V.A. Avetisov, A.Kh. Bikulov, A.P. Zubarev, Ultrametricity as a basis for organization of protein molecules: CO binding to myoglobin, *Vestn. Samar. Gos. Tekhn. Univ. Ser. Fiz.-Mat. Nauki*, 1(30) (2013) 315-325. <https://doi.org/10.14498/vsgtu1154> 1
- [26] A.Kh. Bikulov, & A.P. Zubarev, Ultrametric theory of conformational dynamics of protein molecules in a functional state and the description of experiments on the kinetics of CO binding to myoglobin, *Physica A: Statistical Mechanics and its Applications* 583 (2021) 126280-1–126280-18. <https://doi.org/10.1016/j.physa.2021.126280> 1
- [27] A.H. Shaib, et al. One-step nanoscale expansion microscopy reveals individual protein shapes, *Nature Biotechnology* 43 (2024) 1539-1547. <https://doi.org/10.1038/s41587-024-02431-9> 1
- [28] B. Velikson, J. Basile, T. Garel, H. Orland, Structural and ultrametric properties of (L-alanine)<sub>20</sub>, *Macromolecules* 26 (18) (1993) 4791–4799. <https://doi.org/10.1021/ma00070a010> 1

- [29] R. Scalco, A. Caffisch, Ultrametricity in protein folding dynamics, *Journal of Chemical Theory and Computation* 8 (5) (2012) 1580-1588. <https://doi.org/10.1021/ct3000052> 1
- [30] M. Mele, R. Covino, R. Potestio, Information-theoretical measures identify accurate low-resolution representations of protein configurational space, *Soft Matter* 18 (2022) 7064-7074. <https://doi.org/10.1039/d2sm00636g> 1
- [31] K.A. Dill, Theory for the folding and stability of globular proteins, *Biochemistry* 24 (1985) 1501–1509. <https://doi.org/10.1021/bi00327a032>
- [32] N. Metropolis, A.W. Rosenbluth, M.N. Rosenbluth, A.H. Teller, E. Teller, Equation of state calculations by fast computing machines, *J. Chem. Phys.* 21 (1953) 1087-1092. <https://doi.org/10.1063/1.1699114> 1
- [33] M.E.J. Newman, G.T. Barkema, *Monte Carlo Methods in Statistical Physics*, Oxford University Press, 1999. 1
- [34] A.P. Zubarev, On stochastic generation of ultrametrics in high-dimensional Euclidean spaces, *p-Adic Numbers, Ultrametric Analysis, and Applications* 6 (2) (2014) 155-165. <https://doi.org/10.1134/S2070046614020046> 1
- [35] A.P. Zubarev, On the ultrametric generated by random distribution of points in Euclidean spaces of large dimensions with correlated coordinates, *Journal of Classification* 34 (3) (2017) 366-383. <https://doi.org/10.1007/s00357-017-9236-8> 1